Applications of Wang-Landau sampling to determine phase equilibria in complex fluids

Applications of Wang-Landau sampling to determine phase equilibria in complex fluids

Georg Ganzenmüller and Philip J. Camp

Citation: J. Chem. Phys. **127**, 154504 (2007); doi: 10.1063/1.2794042
View online: http://dx.doi.org/10.1063/1.2794042
View Table of Contents: http://jcp.aip.org/resource/1/JCPSA6/v127/i15
Published by the AIP Publishing LLC.

Applications of Wang-Landau sampling to determine phase equilibria in complex fluids

Georg Ganzenmüller[a] and Philip J. Camp[b]
School of Chemistry, University of Edinburgh, West Mains Road, Edinburgh EH9 3JJ, United Kingdom

(Received 31 May 2007; accepted 11 September 2007; published online 16 October 2007)

Applications of the Wang-Landau algorithm for simulating phase coexistence at fixed temperature are presented. The number density is sampled using either volume scaling or particle insertion/deletion. The resulting algorithms, while being conceptually easy, are of comparable efficiency to existing multicanonical methods but with the advantage that neither the chemical potential nor the pressure at phase coexistence has to be estimated in advance of the simulation. First, we benchmark the algorithm against literature results for the vapor-liquid transition in the Lennard-Jones fluid. We then demonstrate the general applicability of the algorithm by studying vapor-liquid coexistence in two examples of complex fluids: charged soft spheres, which exhibit a transition similar to that in the restricted primitive model of ionic fluids, being characterized by strong ion pairing in the vapor phase; and Stockmayer fluids with high dipole strengths, in which the constituent particles aggregate to form chains, and for which the very existence of a transition has been widely debated. Finally, we show that the algorithm can be used to locate a weak isotropic-nematic transition in a fluid of Gay-Berne mesogens. © *2007 American Institute of Physics*. [DOI: 10.1063/1.2794042]

I. INTRODUCTION

The phase behavior of fluids is of general importance in many fields of science and engineering. Monte Carlo (MC) methods are particularly well suited for simulating phase transitions in simple models.[1] While standard simulation methods are often sufficient for sampling coexisting phases with comparable and low densities, they cannot be used to probe directly the phase coexistence region well below the critical temperature where the transition is strong, i.e., where there is a large difference in order parameter between the coexisting phases. The problem arises mainly from the large free-energy barrier separating the coexisting phases, which is associated with forming an interface within the simulation cell. Many new algorithms have been devised to overcome or circumvent this barrier. Multicanonical sampling[2] biases the simulation such that the free-energy barrier is canceled out, allowing uniform sampling of the coexisting phases and all intermediate states. Parallel tempering[3,4] accelerates MC sampling by exchanging thermodynamic parameters among a large number of replicas being considered simultaneously, thus allowing the exploration of a path "around" the barrier, rather than "through" the barrier. In recent years, huge advances in uniform (or flat-histogram) sampling methodologies have been made. Abreu and Escobedo provide a very general framework for conducting uniform sampling of arbitrary order parameters in a variety of ensembles.[5] Such order parameters are usually mechanically extensive variables like the energy, the volume, or the number of particles. In Metropolis importance sampling MC, statistical expectation values for these order parameters are computed as simple arithmetic averages of simulation measurements. In contrast, expectation values from flat-histogram simulations have to be computed by properly reweighting the simulation measurements. The reweighting step corresponds to dividing out the biased probability density which led to uniform sampling in the first place, and then multiplying by the probability density appropriate to the specific ensemble for which we wish to know the result. In Ref. 5 it is demonstrated that reweighting is not only possible for mechanical, extensive variables but also for structural, intensive properties such as radial distribution functions. In order to sample an order parameter uniformly, one needs to know the weights which yield a flat histogram; these are often referred to as the multicanonical (MUCA) weights. As we will show below, knowledge of this distribution is tantamount to knowing the free energy as a function of order parameter, which of course is unknown *a priori*. However, iterative schemes can be employed to map out the free-energy profile and build up the biasing distribution during the course of a simulation. The specific scheme for obtaining the weights is what distinguishes the many types of flat-histogram sampling methods currently available. These schemes can be broadly divided into two classes: "visited-states" and "transition-probability" methods. The original MUCA formulation by Berg and Neuhaus,[2] entropic sampling,[6] and the relatively new Wang-Landau (WL) (or "density-of-states") sampling[7–10] belong to the visited-states class. One way to employ transition-probability data is Bennett's acceptance ratio method.[11,12] Recent examples of flat-histogram sampling based on transition-matrix (TM) data appear in Refs. 5 and 12–14. For a general review of flat-histogram techniques, see Ref. 15.

Much of the above-cited work deals with the general theoretical concepts and algorithmic details of uniform sampling, and thus mainly considers lattice models or the Lennard-Jones fluid. In this article, we focus on determining

[a]Electronic mail: g.ganzenmueller@ed.ac.uk
[b]Electronic mail: philip.camp@ed.ac.uk

vapor-liquid coexistence in complex fluids which are difficult to simulate. We use the WL algorithm in order to facilitate flat-histogram sampling of the number density ρ, which is the appropriate order parameter for vapor-liquid phase transitions (at least away from the critical point). This is accomplished by working either in the isothermal-isobaric ensemble and performing changes in the volume V, or in the grand-canonical ensemble by changing the number of particles N. If traditional simulation techniques like parallel tempering or multicanonical sampling with fixed weights are used, the pressure or chemical potential for phase coexistence has to be known in advance to enable repeated traversals between liquid and vapor phases so that accurate statistics can be accumulated in the course of a single simulation. The search for suitable parameters is often a tedious task and requires many small trial-and-error simulations before actual production runs can be started. Histogram reweighting can be used subsequently to fine-tune the conditions for coexistence.[16] In contrast, algorithms which determine the weights iteratively do not suffer from this drawback.

The central idea of the WL algorithm is to perform a random walk in one or more thermodynamic variables, and to bias the simulation in order to effect uniform sampling of those variables, i.e., to obtain "flat histograms." In the case of sampling the number of particles N and the potential energy E at fixed volume V, the required biasing function is a density of potential-energy states $\Omega(N,V,E)$ which can be determined by a process of iteration (to be detailed later). Once $\Omega(N,V,E)$ is known, all thermodynamic functions can be determined at any temperature T for which the dominant values of N and E have been sampled adequately. In Refs. 8 and 9 the vapor-liquid coexistence envelopes for small systems of Lennard-Jones spheres have been obtained using the WL approach. In spite of the tempting prospect of generating the whole phase coexistence envelope from one single simulation, this approach is not of general utility because for even the smallest systems ($N \lesssim 100$) it requires vast amounts of CPU time to determine $\Omega(N,V,E)$ over the full ranges of N and E. This led the authors of Ref. 8 to conclude that multicanonical sampling with fixed weights is more effective if both N and E are to be sampled at the same time.

In this article, we use the WL approach to simulate phase coexistence at fixed temperature, thus sampling only the number density. This sampling can be achieved by changing either the volume with fixed N or the number of particles with fixed V. The scheme has already been suggested by Yan *et al.*, who used it to sample N at fixed V and T in preparation for a full density-of-states sampling of N and E.[9] In Ref. 13, Errington used a closely related TM scheme to compute the vapor-liquid coexistence envelope of the Lennard-Jones fluid, both by varying N with fixed V (grand-canonical ensemble) and V with fixed N (isothermal-isobaric ensemble). Irrespective of whether the TM approach or the WL scheme is employed, essential features of the simulations remain unchanged; the overall aim is to achieve uniform sampling of the order parameter over a desired range spanning two phases at coexistence. In general, the TM approach and multicanonical techniques have been demonstrated to yield very precise results (at least for simple systems, such as the Lennard-Jones fluid), with the only minor drawback being that rough estimates for the chemical potential or pressure at coexistence have to be determined in short preliminary simulations in order that full sampling of the density can be achieved in an efficient manner. On the other hand, WL achieves broad sampling of the density in a relatively short time (again, for simple systems), although the precision of the final results is not so good as with the TM approach. One of the main objectives of this work is to explore "difficult" phase transitions in complex fluids. We demonstrate that the WL approach can work where other simulation techniques appear to fail; a specific example discussed in this paper is the vapor-liquid transition in Stockmayer fluids with high dipole strengths. In this case, the very existence of the transition has been called in to question. The main requirement is that the coexisting phases can be sampled adequately in a finite amount of CPU time; we therefore employ the WL algorithm.

In this paper we first compare the accuracy of the WL methods against high-quality data already available for the Lennard-Jones fluid. We then demonstrate the broad applicability of our sampling scheme by attacking some difficult transitions, namely the vapor-liquid transitions of charged soft spheres and of the strongly dipolar Stockmayer fluid, and the isotropic-nematic transition of Gay-Berne mesogens. The rest of this article is organized as follows. First, we give a general outline of flat-histogram sampling. We then derive equations for conducting such sampling in the canonical, grand-canonical, and isothermal-isobaric ensembles, and then detail the implementation within the WL scheme. Following that, we present specific details and results of our calculations on the Lennard-Jones fluid, charged soft spheres, the Stockmayer fluid, and the Gay-Berne model. We finish by discussing the efficiency of the WL variants and by addressing future possible improvements to these sampling schemes.

II. METHODOLOGY

The aim of this section is to outline a general method with which partition functions (up to multiplicative constants) and thermodynamic properties (up to additive constants) can be determined from a flat-histogram MC simulation. The discussion will begin with generalities, and then move on to the specific details in each of the most common statistical mechanical ensembles. Consider an ensemble in which an extensive thermodynamic variable X is allowed to fluctuate; in the present work X will correspond either to the number of particles N, the volume V, or the instantaneous *potential* energy E. For simplicity, the discussion will apply to N identical particles in a cubic box of length L. A specific configuration of N particles will be denoted by Γ, shorthand for the set of scaled coordinates on a unit cube $\{\mathbf{s}_1,\ldots,\mathbf{s}_N\}$, i.e., the actual position vector of particle i is $\boldsymbol{r}_i = L\mathbf{s}_i$. If $p(\Gamma,X)$ is the probability distribution of Γ and X, then the distribution of X is given by

$$p(X) = \int p(\Gamma, X) \mathrm{d}\Gamma. \tag{1}$$

In flat-histogram methods, a biased distribution is sought that leads to uniform sampling of the extensive variable(s). Clearly, the appropriate biased distribution which leads to a uniform sampling of X is

$$p_{\mathrm{bias}}(\Gamma, X) = \frac{p(\Gamma, X)}{p(X)}, \tag{2}$$

for then $p_{\mathrm{bias}}(X) = \int p_{\mathrm{bias}}(\Gamma, X)\mathrm{d}\Gamma = 1$. In a MC scheme, if moves from an old state (Γ_o, X_o) to a new state (Γ_n, X_n) are *attempted* without bias, then the detailed balance condition is[17]

$$p_{\mathrm{bias}}(\Gamma_o, X_o)\mathrm{acc}(o \to n) = p_{\mathrm{bias}}(\Gamma_n, X_n)\mathrm{acc}(n \to o), \tag{3}$$

where $\mathrm{acc}(o \to n)$ is the probability of accepting a trial move from state o to state n. The Metropolis solution of Eq. (3) is

$$\mathrm{acc}(o \to n) = \min\left[1, \frac{p_{\mathrm{bias}}(\Gamma_n, X_n)}{p_{\mathrm{bias}}(\Gamma_o, X_o)}\right]. \tag{4}$$

In the following sections, it is shown explicitly how $p_{\mathrm{bias}}(\Gamma, X)$ is related to partition functions. Of course, the function $p(X)$ is not known in advance, but must be determined iteratively by some scheme. One available method is Wang-Landau sampling, which is described in Sec. II E.

A. Uniform sampling of *E*: The canonical ensemble

To obtain a biased simulation that samples the potential energy $E = U(\Gamma)$ uniformly for fixed N and V, consider the canonical (NVT) ensemble. The Boltzmann distribution for Γ is

$$p(\Gamma) = \frac{V^N \exp[-\beta U(\Gamma)]}{N!\,\Lambda^{3N} Q(N, V, T)}, \tag{5}$$

where $\Lambda = \sqrt{h^2/2\pi m k_B T}$ is the de Broglie thermal wavelength, and

$$Q(N, V, T) = \frac{V^N}{N!\,\Lambda^{3N}} \int \exp[-\beta U(\Gamma)]\mathrm{d}\Gamma \tag{6}$$

is the canonical partition function. $E = U(\Gamma)$ is a function of the particle coordinates, and so the energy distribution is

$$p(E) = \int p(\Gamma)\,\delta(U(\Gamma) - E)\mathrm{d}\Gamma = \frac{V^N \Omega(N, V, E)\exp(-\beta E)}{N!\,\Lambda^{3N} Q(N, V, T)}, \tag{7}$$

where $\Omega(N, V, E) = \int \delta(U(\Gamma) - E)\mathrm{d}\Gamma$ is a density of potential-energy states. Inserting Eqs. (5) and (7) into Eq. (2) yields the biased distribution

$$p_{\mathrm{bias}}(\Gamma, E) = \frac{1}{\Omega(N, V, E)}, \tag{8}$$

and so

$$\mathrm{acc}(o \to n) = \min\left[1, \frac{\Omega(N, V, E_o)}{\Omega(N, V, E_n)}\right]. \tag{9}$$

Hence, the temperature disappears from the sampling scheme, and the biasing function required to achieve uniform sampling of E is the density of potential-energy states, with N and V fixed.

B. Uniform sampling of *V*: The isothermal-isobaric ensemble

To obtain a biased simulation that samples the volume V uniformly for fixed N and T, consider the isothermal-isobaric (NPT) ensemble. The joint Boltzmann distribution for Γ and V is

$$p(\Gamma, V) = \frac{V^N \exp[-\beta U(\Gamma) - \beta P V]}{N!\,\Lambda^{3N} Q(N, P, T)}, \tag{10}$$

where

$$Q(N, P, T) = \int_0^\infty Q(N, V, T)\exp(-\beta P V)\mathrm{d}V \tag{11}$$

is the isothermal-isobaric partition function. The volume distribution is

$$p(V) = \int p(\Gamma, V)\mathrm{d}\Gamma = \frac{Q(N, V, T)\exp(-\beta P V)}{Q(N, P, T)}. \tag{12}$$

Substituting Eqs. (10) and (12) into Eq. (2) leads to

$$p_{\mathrm{bias}}(\Gamma, V) = \frac{V^N \exp[-\beta U(\Gamma)]}{N!\,\Lambda^{3N} Q(N, V, T)}, \tag{13}$$

and so

$$\mathrm{acc}(o \to n) = \min\left[1, \frac{Q(N, V_o, T)}{Q(N, V_n, T)} \cdot \frac{V_n^N \exp[-\beta U(\Gamma_n)]}{V_o^N \exp[-\beta U(\Gamma_o)]}\right]. \tag{14}$$

Hence, the pressure disappears from the scheme, and the biasing function required to achieve uniform sampling of V is the canonical partition function expressed as a function of V, with N and T fixed. In applications, it may be more convenient to sample $\ln V$ uniformly rather than V, in which case the factors of V^N in Eq. (14) should be replaced with V^{N+1}.

C. Uniform sampling of *N*: The grand-canonical ensemble

To obtain a biased simulation that samples the particle number N uniformly for fixed V and T, consider the grand-canonical (μVT) ensemble. The joint Boltzmann distribution for Γ and N is

$$p(\Gamma, N) = \frac{V^N \exp[\beta \mu N - \beta U(\Gamma)]}{N!\,\Lambda^{3N} Q(\mu, V, T)}, \tag{15}$$

where

$$Q(\mu, V, T) = \sum_{N=0}^{\infty} Q(N, V, T)\exp(\beta \mu N) \tag{16}$$

is the grand-canonical partition function. The particle-number distribution is

$$p(N) = \int p(\Gamma,N)\mathrm{d}\Gamma = \frac{Q(N,V,T)\exp(\beta\mu N)}{Q(\mu,V,T)}. \tag{17}$$

Substituting Eqs. (15) and (17) into Eq. (2) yields

$$p_{\mathrm{bias}}(\Gamma,N) = \frac{V^N \exp[-\beta U(\Gamma)]}{N!\,\Lambda^{3N} Q(N,V,T)}, \tag{18}$$

and so

$$\mathrm{acc}(o \to n) = \min\left[1, \frac{Q(N_o,V,T)}{Q(N_n,V,T)} \cdot \frac{V^{N_n} N_o!\,\Lambda^{3N_o}\exp[-\beta U(\Gamma_n)]}{V^{N_o} N_n!\,\Lambda^{3N_n}\exp[-\beta U(\Gamma_o)]}\right]. \tag{19}$$

Hence, the chemical potential disappears from the scheme, and the biasing function required to achieve uniform sampling of N is the canonical partition function expressed as a function of N with V and T fixed. Equation (19) is equivalent to Eqs. (15) and (16) of Ref. 9.

D. Uniform sampling of *N* or *V*, and *E*

Of course, the simple prescription outlined in this section should also give the correct MC rules for sampling the joint density of states of number density and potential energy. In the grand-canonical ensemble

$$p(N,E) = \int p(\Gamma,N)\,\delta(U(\Gamma) - E)\mathrm{d}\Gamma = \frac{V^N \Omega(N,V,E)\exp(\beta\mu N - \beta E)}{N!\,\Lambda^{3N} Q(\mu,V,T)}, \tag{20}$$

and so $p_{\mathrm{bias}}(\Gamma,N,E) = 1/\Omega(N,V,E)$. A scheme for sampling V and E can also be derived. In the isothermal-isobaric ensemble

$$p(V,E) = \int p(\Gamma,V)\,\delta(U(\Gamma) - E)\mathrm{d}\Gamma = \frac{V^N \Omega(N,V,E)\exp(-\beta E - \beta P V)}{N!\,\Lambda^{3N} Q(N,P,T)}, \tag{21}$$

and so $p_{\mathrm{bias}}(\Gamma,V,E) = 1/\Omega(N,V,E)$. These are the well-known results employed in Refs. 7–10.

E. Wang-Landau scheme

It remains to specify how to obtain the required biasing functions (Ω or Q). In all cases discussed above, the partition function of the ensemble to be sampled is given by a Laplace transform of the biasing function. In the following we consider the canonical ensemble, but the extension to other ensembles is straightforward. The canonical partition function is given by

$$Q(N,V,T) = \frac{V^N}{N!\,\Lambda^{3N}} \int \Omega(N,V,E)\exp(-\beta E)\mathrm{d}E. \tag{22}$$

Because Laplace transforms are unique, knowledge of the biasing function implies knowledge of the ensemble partition function, which is of course just the quantity we want during the simulation. It is here where the WL algorithm[7] comes in, as it provides a route to finding $\Omega(N,V,E)$ in a self-consistent way. At the beginning of the simulation, an initial guess is made, e.g., $\Omega(N,V,E) = \text{constant}\ \forall E$. As the simulation proceeds, the current estimates of $\Omega(N,V,E)$ are used for determining whether a trial move is accepted or not. Whenever a specific energy E_i is sampled, $\Omega(N,V,E_i)$ is updated by the operation $\Omega(N,V,E_i) \to f \times \Omega(N,V,E_i)$, where f is an arbitrary convergence factor greater than unity. Also, a histogram of visited energies $H(E_i)$ is kept during the course of the simulation. Due to the dynamic updating of $\Omega(N,V,E)$, the simulation is always pushed away from the current E in the next move and $H(E)$ will eventually become flat. When this is the case f is reduced, e.g., by letting $f = \sqrt{f}$ and $H(E)$ is reset to zero. The simulation is run until f reaches a value f_{min} which is arbitrarily close to unity so that future updates of $\Omega(N,V,E)$ are negligible. The canonical partition function, and hence the Helmholtz free energy F, can be obtained by substituting for $\Omega(N,V,E)$ in Eq. (22) and then using the fundamental relation $\beta F = -\ln Q(N,V,T)$. F is determined up to an additive constant, which is sufficient for locating the conditions for phase coexistence (equal chemical potential and pressure). Even though there is substantial freedom in the parameters of this recipe, like the initial choice of f and the criterion for judging whether $H(E)$ is "flat," the convergence of the WL algorithm has been formally proved.[18]

For the grand-canonical and isothermal-isobaric ensembles the principle is exactly the same. The weights are now given by the canonical partition functions $Q(N,V,T)$, which are set to a constant value at the beginning of the simulation and are dynamically updated with the current state given by N or V, according to the scheme outlined above. In the following, we will abbreviate the grand-canonical and the isothermal-isobaric WL schemes as GCWL and *NPT*WL, respectively. The methodological advantage over traditional simulation techniques like multicanonical sampling is that, without prior specification of coexistence parameters, the whole equation of state (pressure as a function of density) is obtained from a single simulation. A phase transition is most easily located by varying the external field (pressure or chemical potential) until a peak in the compressibility is found. The value of μ or P for phase coexistence is then further refined by tuning the bimodal number density probability distribution until both peaks have equal area.

III. SIMULATION RESULTS

A. Lennard-Jones fluid

In order to assess the performance of the GCWL and *NPT*WL approaches, we compare results against existing high-quality grand-canonical MC (GCMC) TM data[13,19] for the Lennard-Jones potential,

$$u(r_{ij}) = 4\epsilon\left[\left(\frac{\sigma}{r_{ij}}\right)^{12} - \left(\frac{\sigma}{r_{ij}}\right)^{6}\right], \tag{23}$$

truncated at $r_{ij}=3\sigma$. Following Ref. 13, GCWL simulations were run at exactly the same system size, i.e., $V=512\sigma^3$, and with the usual long-range corrections applied.[20] For the *NPT*WL calculations we chose $N=216$. The density ranges sampled during the WL simulations were as follows: with GCWL, $0\leq N\leq 454$ corresponding to $0\leq\rho^*=N\sigma^3/V\leq 0.89$; with *NPT*WL, $10^{-3}\leq\rho^*\leq 0.9$. While there is a natural discretization of $Q(N,V,T)$ if the particle number is varied (as in GCWL), this is not the case for the continuous variable V (as in *NPT*WL). Therefore, an arbitrary binning scheme has to be employed which is fine enough to capture the curvature of $p(V)$, but does not use too many bins because otherwise computational efficiency deteriorates. We decided to use 100 histogram bins with a uniform spacing in $\ln V$, and in the *NPT*WL update scheme we performed changes in $\ln V$ with a maximum step size of twice the bin width. For this model and the other simulations reported below, f started from $\ln f=1$ and a run was considered converged when it reached $\ln f=10^{-8}$ for GCWL and $\ln f=10^{-5}$ for *NPT*WL. f was reduced according to the rule $f=\sqrt{f}$ as soon as all entries in H had been visited at least 1000 times for GCWL and 500 times for *NPT*WL. Maximum displacements for single-particle moves were adjusted to give acceptance ratios of 50%. The time required to converge the simulations was 4 and 12 h for GCWL and *NPT*WL, respectively. All simulation times reported here are for Intel Xeon processors clocked at 2.4 GHz.

In the case of GCWL, coexisting vapor and liquid densities were obtained from the converged estimates of $Q(N,V,T)$ by integrating the low and high-density branches in the particle number probability distribution $p(N)$, with the chemical potential adjusted such that both branches have equal area. If the boundary so determined is at $N=N_b$, then the average densities in the vapor ($N<N_b$) and liquid ($N>N_b$) branches are given by

$$\langle\rho_{\mathrm{vap}}\rangle = \frac{\Sigma_{N<N_b}(N/V)Q(N,V,T)e^{\beta\mu N}}{\Sigma_{N<N_b}Q(N,V,T)e^{\beta\mu N}},$$

$$\langle\rho_{\mathrm{liq}}\rangle = \frac{\Sigma_{N>N_b}(N/V)Q(N,V,T)e^{\beta\mu N}}{\Sigma_{N>N_b}Q(N,V,T)e^{\beta\mu N}}. \tag{24}$$

The boundary N_b between vapor and liquid peaks was identified with the value of N where $p(N)$ is at a minimum. In the case of *NPT*WL, the procedure is completely analogous but with N replaced by V, and sums replaced by integrals,

$$\langle\rho_{\mathrm{vap}}\rangle = \frac{\int_{V_b}^{\infty}(N/V)V^N Q(N,V,T)e^{-\beta PV}\mathrm{d}V}{\int_{V_b}^{\infty}V^N Q(N,V,T)e^{-\beta PV}\mathrm{d}V},$$

$$\langle\rho_{\mathrm{liq}}\rangle = \frac{\int_{0}^{V_b}(N/V)V^N Q(N,V,T)e^{-\beta PV}\mathrm{d}V}{\int_{0}^{V_b}V^N Q(N,V,T)e^{-\beta PV}\mathrm{d}V}. \tag{25}$$

Coexistence results are shown in Fig. 1, with a maximum deviation between WL and TM data[13,19] of 1.0% and an average deviation of 0.4%. The good agreement of the coexistence densities is also reflected in rough estimates of the critical parameters, obtained by fitting the universal equation

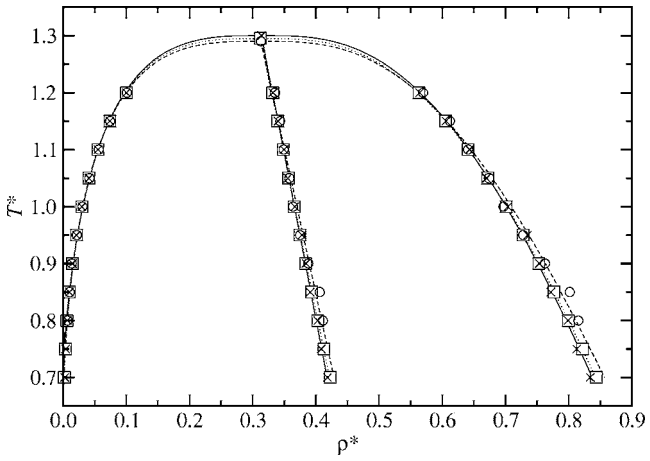

FIG. 1. Vapor-liquid coexistence envelopes for the Lennard-Jones fluid from simulations (points) and fits to the simulation points using Eq. (26) (lines): transition matrix MC (Refs. 13 and 19): squares and dotted lines; GCWL: crosses and solid lines; *NPT*WL: circles and dashed lines.

$$\rho_{\pm} = \rho_c + At \pm Bt^{\beta}, \tag{26}$$

where $t=|T-T_c|/T_c$ and $\beta=0.3265$ is the 3D Ising order-parameter exponent.[21] The apparent critical temperatures and densities are $T_c^*=k_BT_c/\epsilon=1.300(4)$ and $\rho_c^*=0.314(1)$ from GCWL, and $T_c^*=1.290(6)$ and $\rho_c^*=0.313(4)$ from *NPT*WL. These are to be compared with fits to TM data:[13,19] $T_c^*=1.2950(6)$ and $\rho_c^*=0.3125(8)$. Estimates of the uncertainties in the last decimal places are given in brackets; these were taken from the fitting errors and are therefore underestimated compared to the true statistical error.

B. Charged soft spheres

While there have been a number of publications on the WL simulation of phase coexistence in fluids, almost all of these have been applied to simple systems like the Lennard-Jones potential. In this study, we aim to show the general applicability of WL sampling by applying the method to complex fluids. The restricted primitive model (RPM) is one such complex fluid. It consists of an equimolar mixture of hard spheres with charges $\pm q$ and equal diameters σ_{HS}. The vapor-phase structure is characterized by the strong association of oppositely charged ions to form dumbbells.[22,23] After a significant number of intensive simulation studies, the location of the critical point and the universality class (Ising) have been established unambiguously.[24,25] Such systems are much harder to simulate than the Lennard-Jones fluid because insertions and deletions have to be effected using pairs of oppositely charged particles in order to maintain charge neutrality; moreover, the favored separation and orientation of each inserted ion pair have to be selected in a biased fashion.[26] Here, we have chosen to use a soft repulsive potential as this facilitates volume scaling moves in the *NPT*WL simulations: if a hard core was used, even an infinitesimal overlap after a volume contraction move would lead to rejection. The interaction potential of the "charged soft spheres" (CSSs) is defined by

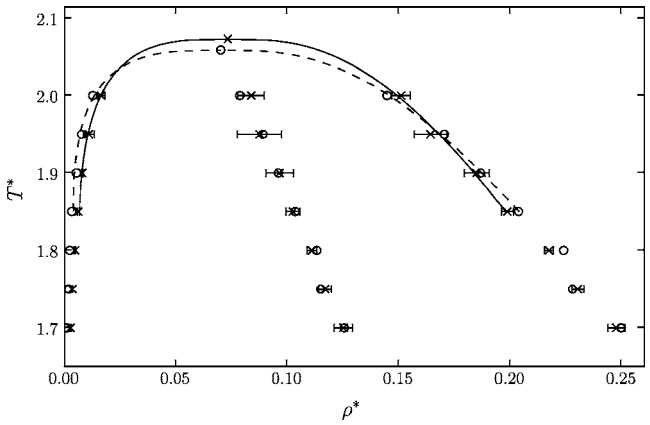

FIG. 2. Vapor-liquid coexistence envelopes for the charged soft sphere fluid from simulations (points) and fits to the simulation points at $T^* \geq 1.85$ using Eq. (26) (lines): GCWL: crosses and solid lines; *NPT*WL: circles and dashed lines.

$$u(r_{ij}) = 4\epsilon\left(\frac{\sigma}{r_{ij}}\right)^{12} + \frac{q_i q_j}{D r_{ij}}, \tag{27}$$

where $D=4\pi\epsilon_0$. Long-range interactions were treated with the Ewald sum and conducting boundary conditions.[20] The soft repulsive potential was cut at $r=2.5\sigma$. In order to compare our results for CSSs with the data available for the RPM, we fixed the reduced charge at $q^*=\sqrt{q^2/D\sigma\epsilon}=\sqrt{48}$, which sets the minimum in the cation-anion potential at $r=\sigma$. The characteristic cation-anion interaction energy is therefore $\epsilon_\pm=-u(\sigma)=44\epsilon$. In order to increase the efficiency of ion-pair insertions and deletions in GCWL simulations, we employed a distance-biased scheme similar to that in Ref. 26, but with a Gaussian biasing function. In GCWL simulations, ion numbers within the fixed volume $V=1000\sigma^3$ varied in the range $0 \leq N/2 \leq 163$, corresponding to ion densities of $0 \leq \rho^* = N\sigma^3/V \leq 0.326$; in *NPT*WL simulations, $N=128$ ions were simulated at densities in the range $10^{-4} \leq \rho^* \leq 0.4$. The WL simulation protocol was the same as that described in Sec. III A.

The coexistence envelopes are shown in Fig. 2. GCWL and *NPT*WL results do not coincide perfectly at all temperatures, but we attribute this to strong finite-size effects connected with the particle number; in GCWL, the number of ion pairs in the vapor phase is very small, whereas in *NPT*WL, the number of ions is fixed. There is a substantial amount of scatter in the data points, which is caused by very broad and flat number-density probability distributions, which in turn complicates the identification of a boundary between liquid and vapor peaks and the subsequent computation of $\langle\rho_{\mathrm{vap}}\rangle$ and $\langle\rho_{\mathrm{liq}}\rangle$. In order to assess the statistical errors, we performed four independent GCWL simulations at each temperature and calculated the statistical uncertainties based on 1 standard deviation; these are shown as horizontal error bars in Fig. 2. It was not possible to improve the accuracy of the individual simulations by requiring a lower f_{min} or a higher minimum count of visited states. Average simulation times for one state point were 4 h with GCWL and 48 h with *NPT*WL.

Rough estimates of the critical temperatures and densities obtained using fits of Eq. (26) are $T_c^*=k_BT_c/\epsilon=2.07(1)$ and $\rho_c^*=0.073(2)$ using GCWL, and $T_c^*=2.059(3)$ and $\rho_c^*=0.070(1)$ using *NPT*WL. Interestingly, the critical density for CSSs obtained here is quite close to the corresponding value for the RPM, $\rho_c^*=\rho\sigma_{\mathrm{HS}}^3=0.0790(25)$.[25] The RPM critical temperature is $k_BT_cD\sigma_{\mathrm{HS}}/q^2=0.05069(2)$,[25] where $q^2/D\sigma_{\mathrm{HS}}$ is the magnitude of the minimum cation-anion energy; the corresponding parameter for CSSs is $\epsilon_\pm=44\epsilon$, leading to an "ionic" critical temperature of $k_BT_c/\epsilon_\pm \simeq 0.047$, which is comparable to that for the RPM. We note that the use of Eq. (26) is questionable because corrections to scaling, and a crossover between classical and Ising regimes, are expected to occur within the range of temperatures being fitted. Nonetheless, the resulting curves look reasonable, and the apparent critical temperatures serve as useful estimates.

We also investigated the possibility of "parallelizing" GCWL simulations by splitting up the interval in N to be sampled, and running separate simulations for each subinterval. This greatly reduces the time required to sample all relevant particle numbers uniformly. A simplistic argument is as follows. Consider an interval in N to be sampled, which we denote by ΔN. If the sampling process is approximated by a one-dimensional random walk in N (which is valid in the limit $f \to 1$), then the sampling time required to visit all states in the interval is proportional to the square of the size of the interval, i.e., $t \propto (\Delta N)^2$. If ΔN is divided into n subintervals of width $\delta N=\Delta N/n$, then the simulation time $t \propto n \times (\delta N)^2 = (\Delta N)^2/n$. This implies that to sample a given range ΔN, the total simulation time is reduced by a factor comparable to the number of subintervals. As an illustration, GCWL simulations of CSSs in the density range $0 \leq \rho^* \leq 0.3$ at $T^*=1.9$ and $V=2197\sigma^3$ were run until $\ln f_{\mathrm{min}}=10^{-6}$. We allowed for an overlap of 10 particles between neighboring subintervals and joined $Q(N,V,T)$ from each subinterval by scaling them such that the midpoints of the overlapping regions were aligned. By simultaneously running simulations over equal subintervals in N, the total simulation times were 9.4, 4.7, and 3.0 h with one, two, and four subintervals, respectively, roughly conforming to a $1/n$ scaling. For a larger system with $V=4096\sigma^3$, the total simulation time required to reach convergence within four equal subintervals was 10.7 h, which is to be compared with the time of 3.0 h for calculations with the same number of subintervals but with half of the volume and hence half the value of ΔN; these results are roughly in line with the suggested $(\Delta N)^2$ scaling.

C. Stockmayer fluid

The phase behavior of strongly dipolar fluids is the subject of a long-running and somewhat controversial debate, which has been comprehensively reviewed several times.[27,28] In brief, de Gennes and Pincus suggested in 1970 that fluids of dipolar hard spheres should exhibit an entirely conventional phase diagram—with vapor, liquid, supercritical fluid, and solid phases—because the leading-order isotropic interaction obtained by a Boltzmann-weighted orientational average of the dipole-dipole interaction potential varies like $-1/r^6$, just like dispersion interactions.[29] The results of computer simulations published in the 1990s suggested otherwise. In the case of dipolar hard spheres, Caillol could find

no evidence of a vapor-liquid transition,[30] although more recent work suggests that this was due to the simulated isotherms being supercritical.[31,32] Another widely studied dipolar system is the Stockmayer fluid, the interaction potential for which is

$$u(r_{ij}) = 4\epsilon\left[\left(\frac{\sigma}{r_{ij}}\right)^{12} - \left(\frac{\sigma}{r_{ij}}\right)^{6}\right] + \frac{\boldsymbol{\mu}_i \cdot \boldsymbol{\mu}_j}{r_{ij}^3} - \frac{3(\boldsymbol{r}_{ij} \cdot \boldsymbol{\mu}_i)(\boldsymbol{r}_{ij} \cdot \boldsymbol{\mu}_j)}{r_{ij}^5}, \tag{28}$$

where $\boldsymbol{\mu}_i$ is the dipole moment on particle i, and the dipole strength $\mu = |\boldsymbol{\mu}_i|$ is the same for all particles. The conventional reduced units are temperature $T^* = k_B T/\epsilon$, number density $\rho^* = \rho\sigma^3$, and dipole strength $\mu^* = \sqrt{\mu^2/\epsilon\sigma^3}$. Gibbs ensemble MC (GEMC) simulations of the Stockmayer potential suggested that the vapor-liquid transition is absent from the phase diagram when $(\mu^*)^2 \gtrsim 24.3$.[33–35] (Note that van Leeuwen and Smit[33] actually simulated a slightly different potential, but one that can be mapped onto the Stockmayer potential;[35] therefore, we only quote equivalent results for the Stockmayer potential.) The disappearance of the vapor-liquid transition has been put down to the formation of chainlike aggregates at low temperatures, with the dipoles in the chains aligned "nose-to-tail."[36] The absence of the transition in some simulations is almost certainly connected with aggregation, but it may be an artifact rather than a real physical effect. The GEMC technique relies on effecting a sufficient number of particle and volume transfers between two different simulation boxes,[37] but the presence of strong aggregation drastically reduces the probability of accepting a simultaneous particle deletion (from one box) and particle insertion (in the other box). In addition, the network of chainlike aggregates severely restricts volume moves. Therefore, it is possible that the disappearance of the vapor-liquid transition in GEMC simulations is actually due to the simulations failing to achieve equilibration and convergence.

Any sort of grand-canonical simulation of strongly dipolar particles is going to be hard work, because of the requirement to execute sufficient numbers of particle insertions and deletions. Nonetheless, we managed to perform GCWL simulations of the Stockmayer fluid with dipole strengths $(\mu^*)^2 = 24$, 27, and 30; the phase behavior at low dipole strengths is already well established.[33,35,38–41] The system volume was $V = L^3 = 1000\sigma^3$, with particle numbers in the range $0 \le N \le 600$. The Lennard-Jones component of the potential was cut off at $L/2$ with no long-range correction applied, while the long-range dipolar interactions were handled using Ewald sums and conducting boundary conditions.[20] GCWL simulations were performed covering intervals of 100 particles plus overlaps of 10 particles with neighboring intervals in order to help splice together the different portions of $Q(N,V,T)$. For $(\mu^*)^2 = 24$, 27, and 30 we performed three, five, and ten independent runs, respectively, at each temperature and averaged the results. Higher dipole strengths required more independent runs due to the difficulty of sampling (by any means) strongly aggregated fluids. We could not simulate higher values of μ^* because the underlying density of states becomes extremely rough due to the presence of system-spanning chains, artificially stabilized by the periodic boundary conditions. This is a problem that we also experienced with simulations of charged hard dumbbells in a recent attack on the transition in dipolar hard spheres.[32] Note that this is a limitation of the finite-size system, and not a failure of the simulation technique *per se*.

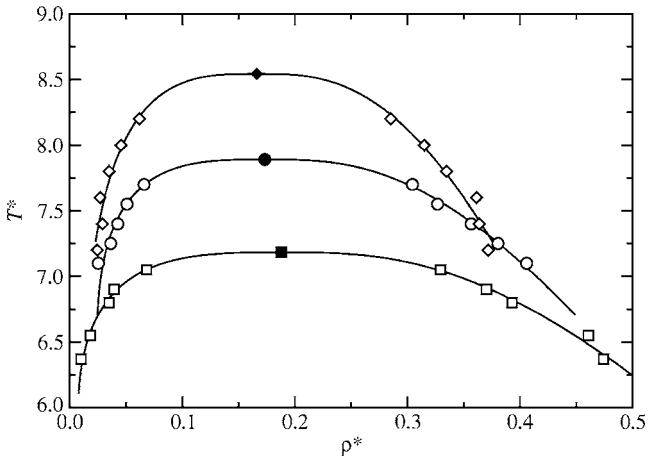

FIG. 3. Vapor-liquid coexistence envelopes for the Stockmayer fluid from GCWL simulations (points) and fits to the simulation points using Eq. (26) (lines): $(\mu^*)^2 = 24$: squares; $(\mu^*)^2 = 27$: circles; $(\mu^*)^2 = 30$: diamonds. The critical points are indicated with filled symbols.

The phase diagrams for systems with $(\mu^*)^2 = 24$, 27, and 30 are shown in Fig. 3; the apparent critical parameters obtained by fits of Eq. (26) are $\{T_c^* = 7.18, \rho_c^* = 0.188\}$, $\{T_c^* = 7.89, \rho_c^* = 0.173\}$, and $\{T_c^* = 8.50, \rho_c^* = 0.165\}$, respectively. In Fig. 4 we compare our critical parameters with a wide selection of GEMC results[33,35,38–40] and the results of recent constant-pressure molecular dynamics simulations.[41] Figure 4(a) shows the inverse of the critical temperature T_c^* plotted against $(\mu^*)^2$. The agreement between our new results and the existing literature results is excellent. It has been noted before[35] that at large values of μ^* the apparent critical temperatures from GEMC simulations vary like $T_c^* \sim (\mu^*)^2$. Accordingly, we fitted all of the available simulation data for $(\mu^*)^2 \ge 10$ with the equation

$$T_c^* = A + B(\mu^*)^2, \tag{29}$$

where $A = 0.937 \pm 0.066$ and $B = 0.2617 \pm 0.0031$. (In Ref. 35, $A = 1.06$ and $B = 0.254$.) This fit is shown as the solid curve in Fig. 4(a). Note that in the limit $\mu^* \to \infty$, the characteristic dipolar temperature $k_B T_c \sigma^3/\mu^2 = T_c^*/(\mu^*)^2$ tends to a finite value of 0.2617.

Figure 4(b) shows the critical densities ρ_c^* plotted against $(\mu^*)^2$. There is good general agreement between our new results and most of the literature values, although it appears that the values of ρ_c^* obtained by Bartke and Hentschke[41] are systematically low, particularly at high values of μ^*. They obtained the phase diagrams and apparent critical points by measuring the equation of state and performing the Maxwell construction, and the long-range dipolar interactions were handled using the reaction-field approach. The source of the discrepancies between their results and the rest of the literature values is unclear.

Our results at $(\mu^*)^2 = 24$ are consistent with earlier work, and following Bartke and Hentschke,[41] we confirm that the

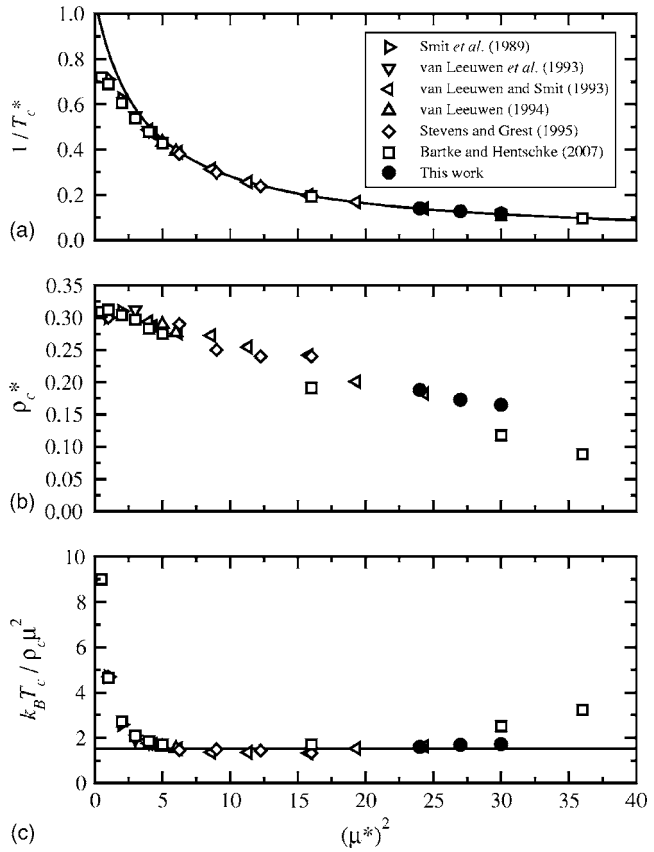

FIG. 4. Critical parameters for the Stockmayer fluid: (a) reciprocal of the critical temperature T_c^*; (b) critical density ρ_c^*; (c) dimensionless ratio $g=k_BT_c/\rho_c\mu^2$. Symbols: Smit *et al.* (Ref. 38): right triangles; van Leeuwen *et al.* (Ref. 39): down triangles; van Leeuwen and Smit (Ref. 33): left triangles; van Leeuwen (Ref. 40): up triangles; Stevens and Grest (Ref. 35): diamonds; Bartke and Hentschke (Ref. 41): squares; this work: filled circles. In (a) the solid curve is the fit $T_c^*=0.937+0.2617(\mu^*)^2$; in (c) the solid horizontal line at $g=1.53$ is the dipolar hard sphere value from Ref. 32.

transition persists at higher dipole strengths, at least up to $(\mu^*)^2=30$. But, as noted above, studying much higher dipole strengths is essentially impossible due to pronounced finite-size effects. In recent work on dipolar hard particles[32] we provided estimates of the critical parameters for dipolar hard spheres with diameter σ and dipole strength μ. In reduced units we found that $k_BT_c\sigma^3/\mu^2=0.153(1)$ and $\rho_c\sigma^3\simeq 0.1$. It would be useful to compare these predictions with the results for the Stockmayer fluid, but mapping one system onto the other is going to be problematic due to the presence of the soft repulsive core in the Stockmayer potential. One might attempt to identify an effective hard-core diameter for the Stockmayer potential, but the anisotropy of the strong, attractive part of the potential will cause problems. Therefore, to effect a meaningful comparison we consider the dimensionless ratio $g=k_BT_c/\rho_c\mu^2$ which does not require any mapping between the different systems. Figure 4(c) shows $g=T_c^*/\rho_c^*(\mu^*)^2$ for the Stockmayer system plotted against $(\mu^*)^2$. Most of the existing literature results suggest that g tends toward some kind of universal, constant value. This value should be characteristic of a purely dipole-driven vapor-liquid transition because, with large values of μ^*, the dipole-dipole interaction must dominate over the Lennard-Jones attraction. The results of Bartke and Hentschke for $(\mu^*)^2\geq 30$ suggest a slight upward trend, but since their critical temperatures appear accurate [from Fig. 4(c)], this feature may be traced to the systematic underestimation of the critical densities apparent in Fig. 4(b). For comparison, in Fig. 4(c) we show the dipolar hard sphere value $g=1.53$ according to Ref. 32. The agreement between most of the literature results for the Stockmayer potential with large values of μ^*, and that for dipolar hard spheres,[32] is excellent and strongly suggests the existence of a vapor-liquid transition driven exclusively by dipole-dipole interactions.

D. Gay-Berne mesogens

The isotropic-nematic ($I-N$) transition in the Gay-Berne model of liquid crystals involves a very small change in density and requires an enormous number of traditional NPT MC simulations to locate accurately.[42–44] The Gay-Berne potential is given by

$$u(\boldsymbol{r}_{ij},\boldsymbol{u}_i,\boldsymbol{u}_j)=4\epsilon(\boldsymbol{r}_{ij},\boldsymbol{u}_i,\boldsymbol{u}_j)\left\{\left[\frac{\sigma_0}{d(\boldsymbol{r}_{ij},\boldsymbol{u}_i,\boldsymbol{u}_j)}\right]^{12}-\left[\frac{\sigma_0}{d(\boldsymbol{r}_{ij},\boldsymbol{u}_i,\boldsymbol{u}_j)}\right]^{6}\right\}, \tag{30}$$

where $\boldsymbol{r}_{ij}$ is the interparticle separation vector, $\boldsymbol{u}_i$ is the orientational vector along the symmetry axis of particle i, and $d(\boldsymbol{r}_{ij},\boldsymbol{u}_i,\boldsymbol{u}_j)=|\boldsymbol{r}_{ij}|-\sigma(\boldsymbol{r}_{ij},\boldsymbol{u}_i,\boldsymbol{u}_j)+\sigma_0$. The quantities $\epsilon(\boldsymbol{r}_{ij},\boldsymbol{u}_i,\boldsymbol{u}_j)$ and $\sigma(\boldsymbol{r}_{ij},\boldsymbol{u}_i,\boldsymbol{u}_j)$ are orientation dependent and proportional to the basic energy and range parameters ϵ_0 and σ_0, respectively. The full expressions are given in Ref. 42, but we note that they depend on two further parameters: κ, which defines the aspect ratio of the (roughly) ellipsoidal molecules; and κ', which sets the ratio between the potential-energy wells for the side-by-side and end-to-end configurations. We focus our attention on the system with $\kappa=3$ and $\kappa'=5$ as studied in previous work.[42–44] Using thermodynamic integration techniques, de Miguel[43] determined the coexistence properties at a temperature $T^*=k_BT/\epsilon_0=1.25$ to be $P^*=P\sigma_0^3/\epsilon_0=5.20$, $\rho_I^*=\rho_I\sigma_0^3=0.3152$, and $\rho_N^*=\rho_N\sigma_0^3=0.3219$.

With the output from a single WL simulation, we can calculate the isothermal compressibility κ_T for a range of pressures. In a finite-size simulation, a peak in κ_T plotted as a function of P can signal a first-order transition between two phases differing in density. Statistical expectation values in the NPT ensemble can be calculated with $Q(N,V,T)$ obtained from NPTWL simulations by numerical integration, as in Eq. (25). The compressibility as a function of P is thus readily obtained from the fluctuation formula,[20]

$$\kappa_T=-\frac{1}{V}\left(\frac{\partial V}{\partial P}\right)_{N,T}=\frac{\langle V^2\rangle-\langle V\rangle^2}{\langle V\rangle k_BT}. \tag{31}$$

In the NPTWL simulations $N=192$ particles were used, and the potential was truncated at $r=4\sigma_0$ with no long-range corrections applied. We did not attempt GCWL simulations for this model because the number of successful particle insertions/deletions is expected to be prohibitively low in the density range $0.25\leq\rho^*\leq 0.35$ considered here. Rotations and translations were performed independently, with maxi-

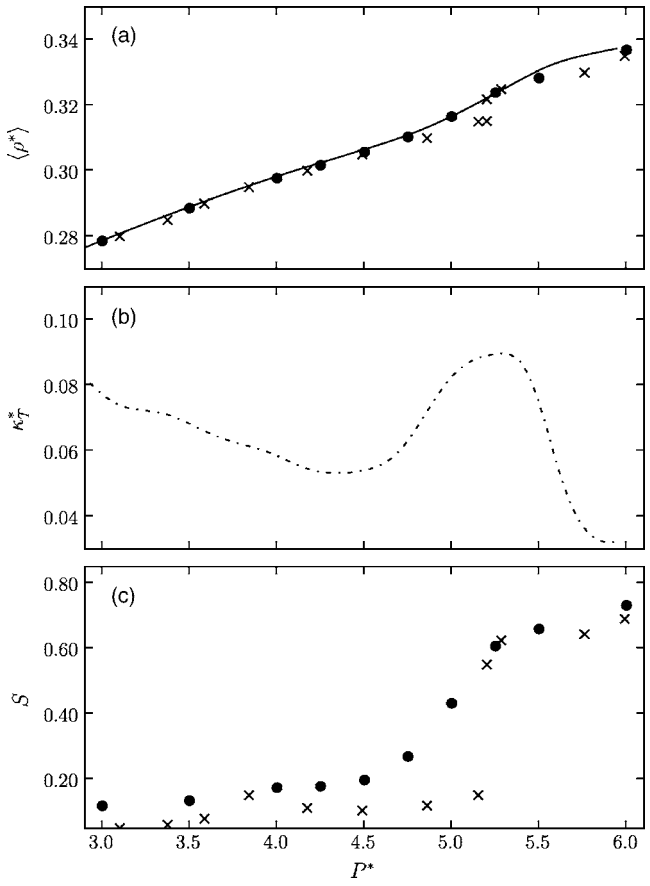

FIG. 5. Results for Gay-Berne mesogens. (a) Equation of state from *NPT*WL simulations (line), standard *NPT*-MC simulations (circles), and canonical molecular dynamics simulations (Refs. 42 and 43) (crosses). (b) Isothermal compressibility $\kappa_T^* = \kappa_T \epsilon_0 / \sigma_0^3$ from *NPT*WL simulations. (c) Nematic order parameter S from standard *NPT*-MC simulations particles (circles) and canonical molecular dynamics simulations (Refs. 42 and 43) (crosses).

mum displacements chosen to give acceptance ratios of approximately 50%.

Results for the equation of state, compressibility, and nematic order parameter S (computed as described in Ref. 45) are shown in Fig. 5, along with available existing canonical molecular dynamics data for $N=500$ particles.[42,43] In addition to the *NPT*WL results, we show the results of our own standard *NPT* simulations with $N=192$ particles. Using the *NPT*WL data, we also calculated $\langle P \rangle$ as a function of ρ (canonical ensemble average) by differentiating $F = -k_B T \ln Q(N,V,T)$ numerically, but the results were indistinguishable from those obtained by computing $\langle \rho \rangle$ as a function of P (*NPT* ensemble average). This is due to the fact that there is no observable "van der Waals" loop in the canonical-ensemble equation of state, and no pronounced hysteresis in the *NPT* results; the absences of these features in simulations of weak $I-N$ transitions have been noted before.[45] A clear peak in κ_T emerges at $P^* \simeq 5.25$ (corresponding to a density $\rho^* \simeq 0.32$), which coincides with the jump in the nematic order parameter. This pressure is quite close to the coexistence pressure $P^*=5.20$ identified by de Miguel.[43] It proved impossible to resolve a bimodal density distribution from the *NPT*WL results at the apparent coexistence pressure because the change in density is too small. In an attempt to improve on this we performed simulations on a slightly larger system with $N=324$, but it was still not possible to observe a bimodal distribution; the peak in κ_T occurs at essentially the same pressure as in the $N=192$ system. The overall agreement between standard *NPT*, *NPT*WL, and canonical molecular dynamics[42,43] simulations is good. Therefore, the *NPT*WL offers a viable route to mapping out the equation of state at fixed temperature from a single simulation—even for dense fluids. A similar simulation has been reported in Ref. 14, where the athermal isotropic-cubatic phase transition of cuboidal particles constructed from hard spheres was probed using a TM-based flat-histogram method. In that case, however, the transition is strongly first order with a difference in density between isotropic and cubatic phases of approximately 10%.

IV. DISCUSSION

In this work, a robust method for determining phase coexistence has been presented. The major advantage over traditional multicanonical MC techniques is that only the density range and temperature at which a transition is expected have to be specified in advance. The effect of the external field, given by the external pressure in the *NPT* ensemble, or the chemical potential in the grand-canonical ensemble, is determined after the simulation has converged and it is thus possible to obtain number-density distributions at arbitrary values of the external field (provided a sufficient range of densities has been sampled in the first place). This also implies that the equation of state for the density range considered can be obtained from a single simulation.

The algorithms described here—GCWL and *NPT*WL—belong to the visited-states class of flat-histogram techniques for determining partition functions. GCWL effects changes in the number density by particle insertions and deletions at fixed volume, while *NPT*WL varies the volume at fixed number of particles. We have applied both algorithms to the vapor-liquid transitions in the Lennard-Jones fluid, charged soft spheres, and Stockmayer fluids with high dipole strengths.

For the Lennard-Jones fluid, we find that both algorithms reproduce existing high-quality transition-matrix data with good accuracy. At strongly subcritical temperatures, one might expect deviations between the GCWL and *NPT*WL results for the vapor coexistence density, because the number of particles in the GCWL simulation is very low compared to that in the *NPT* simulation. However, for the Lennard-Jones fluid, we find that this effect is not significant.

Surprisingly, the coexistence curves for charged soft spheres from GCWL and *NPT*WL simulations are consistent with one another over the entire temperature range considered, but there is a significant amount of statistical scatter. Rough estimates of the critical parameters obtained from fitting an Ising-type scaling law are $T_c^* \simeq 2.06$ and $\rho_c^* = 0.07$. The apparent critical parameters—expressed in "ionic" reduced units—are in good accord with those for charged hard spheres (restricted primitive model).[24,25]

The vapor-liquid coexistence curves for the Stockmayer fluid with high dipole strengths could be generated reliably

using the GCWL approach. Our results—like those of Bartke and Hentschke[41]—indicate that the transition persists well above the critical dipole strength identified by van Leeuwen and Smit.[33] In fact, the apparent disappearance of the transition in GEMC simulations[33–35] is more than likely associated with failures of the simulation methodology. The results at high dipolar strengths compare well with recent data for dipolar hard spheres,[32] supporting the existence of a vapor-liquid transition driven by purely dipolar interactions.

The natural discretization of N renders the GCWL approach computationally more straightforward than NPTWL. Simulation times for GCWL reported here are moderate. In addition, parallelization of the algorithm is simple because the density range can be split into multiple intervals for which independent simulations are performed. The resulting numerical estimates of the canonical partition functions from each subinterval are then scaled so that they match up at the boundaries.[7,8] Preliminary investigations of this approach showed that the total time needed to complete a simulation is reduced by a factor comparable to the number of subintervals. In the light of these results, the application of parallelized GCWL simulations to very large systems is an attractive proposition. Based on these observations, we can recommend using GCWL for locating vapor-liquid transitions.

In general, we observed that it was not possible to reduce errors in vapor and liquid coexistence densities by increasing the primary adjustable parameters in the WL scheme—the final value of the convergence factor and the flatness of the histogram of visited states. It has been noted before that the WL algorithm does not improve on the statistical error after f has reached a certain value.[10] We therefore propose that if very accurate results are required, a combination of GCWL and GCMC with multicanonical biasing could be employed: the required value for the chemical potential and a good guess for the multicanonical bias is obtained from a preliminary GCWL simulation; a multicanonical GCMC simulation can then be run, which also enables the use of histogram reweighting.

The isotropic-nematic transition of Gay-Berne mesogens is only feasible using NPTWL simulations because the packing fraction in the vicinity of the transition is too high to effect particle insertions and deletions. Unfortunately, the transition is so weak that a bimodal density distribution could not be obtained; this property of the isotropic-nematic transition gives rise to problems in other "direct" simulation techniques.[45] Nonetheless, by calculating the compressibility and equation of state from a single simulation, we could locate the transition pressure. Therefore, the NPTWL technique might also find application in the simulation of strong, first-order phase transitions at high densities.

ACKNOWLEDGMENTS

We thank Professor Alexey O. Ivanov and Dr. Sofia S. Kantorovich for discussions on the Stockmayer fluid. The support of the UK Engineering and Physical Sciences Research Council Grant No. EP/D002656/1 is gratefully acknowledged. This work has made use of the resources provided by the EaStCHEM Research Computing Facility, which is partially supported by the eDIKT initiative.

[1] A. Z. Panagiotopoulos, J. Phys.: Condens. Matter **12**, R25 (2000).
[2] B. A. Berg and T. Neuhaus, Phys. Rev. Lett. **68**, 9 (1992).
[3] A. P. Lyubartsev, A. A. Martsinovski, S. V. Shevkunov, and P. N. Vorontsov-Velyaminov, J. Chem. Phys. **96**, 1776 (1992).
[4] Q. Yan and J. J. de Pablo, J. Chem. Phys. **111**, 9509 (1999).
[5] C. R. A. Abreu and F. A. Escobedo, J. Chem. Phys. **124**, 054116 (2006).
[6] J. Lee, Phys. Rev. Lett. **71**, 211 (1993).
[7] F. Wang and D. P. Landau, Phys. Rev. Lett. **86**, 2050 (2001).
[8] M. S. Shell, P. G. Debenedetti, and A. Z. Panagiotopoulos, Phys. Rev. E **66**, 056703 (2002).
[9] Q. Yan, R. Faller, and J. J. de Pablo, J. Chem. Phys. **116**, 8745 (2002).
[10] M. S. Shell, P. G. Debenedetti, and A. Z. Panagiotopoulos, J. Chem. Phys. **119**, 9406 (2003).
[11] C. H. Bennett, J. Comput. Phys. **22**, 245 (1976).
[12] F. A. Escobedo and C. R. A. Abreu, J. Chem. Phys. **124**, 104110 (2006).
[13] J. R. Errington, J. Chem. Phys. **118**, 9915 (2003).
[14] I. D. Gospodinov and F. A. Escobedo, J. Chem. Phys. **122**, 164103 (2005).
[15] Y. Okamoto, J. Mol. Graph. Model. **22**, 425 (2004).
[16] A. M. Ferrenberg and R. H. Swendsen, Phys. Rev. Lett. **61**, 2635 (1988).
[17] D. Frenkel and B. Smit, *Understanding Molecular Simulation: From Algorithms to Applications*, 2nd ed. (Academic, San Diego, 2001).
[18] C. Zhou and R. N. Bhatt, Phys. Rev. E **72**, 025701 (2005).
[19] J. R. Errington, URL: http://www.cstl.nist.gov/srs/LJ_PURE/sattmmc.htm (2003).
[20] M. P. Allen and D. J. Tildesley, *Computer Simulation of Liquids* (Clarendon, Oxford, 1987).
[21] A. M. Ferrenberg and D. P. Landau, Phys. Rev. B **44**, 5081 (1991).
[22] J.-M. Caillol and J.-J. Weis, J. Chem. Phys. **102**, 7610 (1995).
[23] J. C. Shelley and G. N. Patey, J. Chem. Phys. **103**, 8299 (1995).
[24] J.-M. Caillol, D. Levesque, and J.-J. Weis, J. Chem. Phys. **116**, 10794 (2002).
[25] E. Luijten, M. E. Fisher, and A. Z. Panagiotopoulos, Phys. Rev. Lett. **88**, 185701 (2002).
[26] G. Orkoulas and A. Z. Panagiotopoulos, J. Chem. Phys. **101**, 1452 (1994).
[27] P. I. C. Teixeira, J. M. Tavares, and M. M. Telo da Gama, J. Phys.: Condens. Matter **12**, R411 (2000).
[28] C. Holm and J.-J. Weis, Curr. Opin. Colloid Interface Sci. **10**, 133 (2005).
[29] P. G. de Gennes and P. A. Pincus, Phys. Kondens. Mater. **11**, 189 (1970).
[30] J.-M. Caillol, J. Chem. Phys. **98**, 9835 (1993).
[31] P. J. Camp, J. C. Shelley, and G. N. Patey, Phys. Rev. Lett. **84**, 115 (2000).
[32] G. Ganzenmüller and P. J. Camp, J. Chem. Phys. **126**, 191104 (2007).
[33] M. E. van Leeuwen and B. Smit, Phys. Rev. Lett. **71**, 3991 (1993).
[34] M. J. Stevens and G. S. Grest, Phys. Rev. Lett. **72**, 3686 (1994).
[35] M. J. Stevens and G. S. Grest, Phys. Rev. E **51**, 5976 (1995).
[36] J. J. Weis and D. Levesque, Phys. Rev. Lett. **71**, 2729 (1993).
[37] A. Z. Panagiotopoulos, Mol. Phys. **61**, 813 (1987).
[38] B. Smit, C. P. Williams, E. M. Hendriks, and S. W. de Leeuw, Mol. Phys. **68**, 765 (1989).
[39] M. E. van Leeuwen, B. Smit, and E. M. Hendriks, Mol. Phys. **78**, 271 (1993).
[40] M. E. van Leeuwen, Mol. Phys. **82**, 383 (1994).
[41] J. Bartke and R. Hentschke, Phys. Rev. E **75**, 061503 (2007).
[42] E. de Miguel, Phys. Rev. E **47**, 3334 (1993).
[43] E. de Miguel, Mol. Phys. **100**, 2449 (2002).
[44] E. de Miguel and C. Vega, J. Chem. Phys. **117**, 6313 (2002).
[45] P. J. Camp, C. P. Mason, M. P. Allen, A. A. Khare, and D. A. Kofke, J. Chem. Phys. **105**, 2837 (1996).